Title: Multi-decadal warming of Antarctic waters

Authors: Sunke Schmidtko[1,2,*], Karen J. Heywood[1], Andrew F. Thompson[3], Shigeru Aoki[4]

Affiliations:

[1]Centre for Ocean and Atmospheric Sciences, School of Environmental Sciences, University of East Anglia, Norwich, NR4 7TJ, United Kingdom.

[2]Helmholtz Centre for Marine Research - GEOMAR, Düsternbrooker Weg 24, 24105 Kiel, Germany.

[3]Environmental Science and Engineering, California Institute of Technology, Pasadena, California, USA.

[4]Institute of Low Temperature Science, Hokkaido University, Sapporo 060-0819, Japan.

*Correspondence to: sschmidtko@geomar.de

Decadal trends in seawater properties adjacent to Antarctica are poorly known, and mechanisms responsible for such changes are uncertain. Antarctic ice sheet mass loss is largely driven by ice shelf basal melt, which is influenced by ocean-ice interactions and correlated with Antarctic continental Shelf Bottom Water (ASBW) temperature. We document the spatial distribution of long-term large-scale trends in temperature, salinity and core depth over the Antarctic continental shelf and slope. Warming at the seabed in the Bellingshausen and Amundsen Seas is linked to increased heat content and to a shoaling of the mid-depth temperature maximum over the continental slope, allowing warmer, saltier water greater access to the shelf in recent years. Regions of ASBW warming are those exhibiting increased ice shelf melt.

One Sentence Summary:

Decadal trends in Antarctic water mass properties show that pronounced warming on the continental shelf is associated with a warming and shoaling of the offshore temperature maximum.

The Antarctic ice sheet is the largest reservoir of terrestrial ice and a significant contributor to sea level rise in a warming climate (*1*). Massive ice shelf disintegration and rapid acceleration of glacial flow have occurred in recent decades (*2*), or are potentially looming (*3*). These events are generally linked to enhanced basal melt (*4*, *5*), which reduces buttressing and accelerates glacier flow. An increase in basal melt may be linked to stronger sub-ice shelf circulation of Circumpolar Deep Water (CDW). It is not known whether changes in the delivery of warm water to the underside of the ice shelf are caused by increased heat content, increased volume flux responding to changes in wind and buoyancy forcing, or some combination of the two (*6*, *7*). Here we focus on documenting long-term temperature and salinity changes in ocean properties over the continental shelf and slopes.

We refer to the water occupying the sea floor on the Antarctic continental shelf as Antarctic continental Shelf Bottom Water (ASBW), and the temperature minimum layer, representing the remnant of the winter mixed layer, as Winter Water (WW). Atmospheric processes, adjacent water masses, ice shelf and continental freshwater fluxes, and bathymetry dependent cross-shelf water exchange at the shelf break determine the hydrographic properties of ASBW. Hence ASBW is a mixture of CDW, WW and waters originating from continental runoff, ice shelf melting or sea ice formation. Temporal changes in ASBW may represent either changes in formation processes or in properties of source water. ASBW has freshened in the Ross Sea (*8*) and northwest Weddell Sea (*9*), with the former generally linked to enhanced upstream ice shelf melt. Recent research has identified large-scale warming of both CDW north of 60°S (*10*) and Antarctic Bottom Water (AABW) (*11*). Yet, statistically-significant long-term warming of

ASBW has only been observed in localized regions (*12*) and trends in CDW properties over the Antarctic continental slope have not previously been discussed.

Using a comprehensive compilation of observational datasets (Tab.S1) ((*13*), see Methods), we find that temporal trends in ASBW temperature and salinity have a distinct regional pattern (Fig.1). The Bellinghausen Sea and Amundsen Sea shelves show statistically significant warming (0.1-0.3°C decade^{-1},Fig.1C,E) and salinification (0.01-0.04 g kg^{-1} decade^{-1},Fig.1D,F) since the 1990s when sufficient observations became available (Fig.S2). The Ross Sea is freshening (-0.027±0.012 g kg^{-1} decade^{-1}) and the western Weddell Sea reveals a slight cooling (-0.05±0.04°C decade^{-1}) and freshening (-0.01±0.007 g kg^{-1} decade^{-1}); older measurements allow these trends to be calculated from the 1970s. The Cosmonaut Sea is freshening (-0.05±0.03 g kg^{-1} decade^{-1}). These trends agree with the available, but limited, regional observations (*12*). The previously documented regional Ross Sea freshening (*8*) (-0.03 g kg^{-1} decade^{-1}) is within the range of the locally mapped values obtained here (-0.01– -0.05 g kg^{-1} decade^{-1}; Fig.1D). Focusing only on data since the mid 1980s (Fig.1F) produces a more pronounced average Ross Sea freshening (-0.05±0.02 g kg^{-1} decade^{-1}). The freshening trend in the western Weddell Sea shelf changes sign if only data from the 1990s are used (Fig.1E,S10). Freshening is observed in the northwestern Weddell Sea (Fig.1D), although the trend doubles and is similar to reported values if data only from the late 1980s to the mid 2000s are considered (*9*).

Temperature trends are typically uniform across the width of the shelf up to the shelf break. In contrast, salinity trends show a cross-shelf gradient with freshening generally intensified close to the coast (Fig.1D); this is particularly pronounced over the Ross Sea and Weddell Sea

continental shelves. A cross-shelf salinity-trend gradient points to physical processes that induce a larger change in salinity than temperature near the continent. For example, changes in surface melt water run-off and changes in sea ice melting or freezing would be seen primarily in salinity, whereas changes in ocean-induced ice shelf basal melting would be seen in both temperature and salinity; atmospheric cooling would be seen in temperature but not salinity, unless sea ice is formed. While changes in melt water run-off and sea ice formation are consistent with the observed temperature and salinity trends, our analysis cannot distinguish between these mechanisms. Lateral variations of the trend vary according to the time period analyzed. The shoreward intensification of the freshening is significantly stronger when all data are used than when only data since 1990 are used (Fig.1D,S10). This difference may originate in poor data coverage from recent decades (Fig.S1,S2) or indicate multi-annual variability in any combination of processes described above (Fig.1E,F).

We next assess the origins of ASBW property trends (Fig.1C,D) by analyzing changes in the properties and the depth of source water masses: the temperature maximum layer approaching the continental shelf break (CDW core, Fig.2) and the temperature minimum layer (WW, Fig.3). CDW shows statistically significant warming and shoaling in most regions around Antarctica (Figs.2D,F), with trends on the order of 0.1°C decade^{-1} and -30 m decade^{-1} respectively. These values are similar to those of isopycnal heave found further north (*10*) and at depth (*14*). There are few significant changes in CDW salinity close to Antarctica; the most pronounced freshening is observed in the Antarctic Circumpolar Current (ACC) in the Indian Ocean sector, likely owing to variations in front location in regions of large meridional gradients (Fig.2B,E).

In addition to regional changes in water mass properties, changes in the depth of the CDW core also show spatial variability. Deepening of the CDW core only occurs along the northern limb of the Weddell Gyre and in the Cosmonaut Sea (Fig.2F). Areas where the CDW core deepens tend to be correlated with cooling. The strongest shoaling of CDW is found in the Bellingshausen and Amundsen Seas, where temporal shoaling rates locally exceed -50±18 m decade^{-1}. Around the Antarctic margins, the core of CDW typically deepens approaching the continental shelf, as in the Weddell and Ross gyres (Fig.2C,4B). However, in the Bellingshausen and Amundsen Seas, the core of CDW slopes upward approaching the shelf (Fig.4A).

The other water mass present over the shelf and slope is WW (Fig.3). WW is freshening along the southwestern limb of the Ross Gyre and in the western Indian Ocean sector, while WW is becoming saltier in the northwestern Weddell Sea (Fig.3E). Significant shoaling of WW is present in the eastern Indian Ocean sector and Amundsen Sea (Fig.3F). Origins of the salinity changes in WW are likely to differ among regions, including changes to sea-ice concentration caused by ice-motion trends (*15*) and changes to sea-ice concentration caused by increased accumulation of ice-shelf meltwater (*16*).

The trends in Figs. 1, 2 show a link between property changes in ASBW and in CDW over the continental slope. The CDW thermal structure may be broadly categorized into two regimes, shown schematically in Fig. 4: CDW (a) sloping upward or (b) sloping downward towards the shelf break. The Weddell and Ross gyres are subject to a large-scale cyclonic wind stress, leading to strong easterly winds over the shelf break that depresses isotherms (Fig.4B). Cyclonic

wind patterns are also found over the Amundsen and Bellingshausen Seas, but the center of the low pressure systems is found over the continental shelf. Thus, in these regions, weaker easterly or even westerly winds are found at the shelf break, causing upward tilting CDW and enhanced onshore intrusions (*17*, *18*) (Fig.4A). Furthermore, the Bellingshausen and Amundsen Seas do not export a significant volume of AABW and a bottom-intensified along-slope Antarctic Slope Current does not form (Fig.4A).

While warming and shoaling of CDW is present around Antarctica, the regions that have experienced the most intense warming and shoaling are associated with areas where CDW has greater access to the shelf break (Fig.4A). Additionally, in all regions where CDW both slopes upwards towards the shelf break and is shoaling over time, ASBW temperatures are rising. This link suggests that changes occurring to CDW offshore in the Bellingshausen and Amundsen Seas (Figs.2D,F) are more likely to be transmitted onto the shelf and be reflected in regional ASBW properties. To contrast this, in regions where CDW slopes downward towards the shelf break, offshore trends in CDW properties show no correlation to bottom water masses on the continental shelves, e.g. near the Ross, Amery, Filchner and Ronne Ice Shelves (Fig.4B). Thus the continental shelf in the Weddell and Ross Seas are in effect shielded from offshore changes in CDW. The one possible exception, though, is the intense shoaling of CDW in the southern Weddell Sea, which raises questions about the future stability of ASBW temperatures in front of the Filchner and Ronne Ice Shelves (*19*) (Fig.2F,G).

Recent dynamical studies have highlighted the importance of surface forcing on links between offshore and onshore properties. In Ross and Weddell gyre idealized model configurations,

surface forcing by the polar easterlies controls onshore transport of WW and CDW as well as the characteristic slope of mid-depth water masses towards the shelf break (*17*). In the Amundsen Sea, offshore atmospheric anomalies modify the thermal gradient across the continental shelf and under the ice shelf (*18*). Buoyancy forcing may also be critical to long-term trends. A simple balance model (*6*) suggests that regional properties are largely set by atmospheric patterns of heating and cooling, but changes in ASBW may depend on the penetration depth of convection. Finally, over the continental slope, mesoscale variability plays a critical role in setting temperature distributions and is sensitive to changes in wind forcing (*20*). It is critical to note that these dynamical processes occur at scales that are necessarily smoothed by our analysis. However, the large-scale trends point to key regions that require more intense analysis through high-resolution modelling with improved bathymetric data to determine the mechanistic cause of these changes.

Since ice shelf melting and ice sheet collapse depend on the delivery of warm water by ocean currents, ice sheet predictability requires accurate estimates of oceanic heat transport. Shoaling CDW has the potential to significantly increase this heat transport, and must be represented in climate models for future ice shelf predictions. Current climate models still have limitations in Southern Ocean mixed layer processes (*21*) and are thus unlikely to represent WW and the underlying CDW shoaling correctly. In addition to onshore transport, capturing changes in exported AABW properties is also critical for modelling the global circulation. ASBW salinity changes in AABW formation regions, like the Weddell and Ross Seas (Fig.1D), resemble the observed freshwater changes in AABW around Antarctica (*14*, *22*). AABW has freshened in the

Indian (*22*) and Pacific sectors, and to a lesser extent in the Atlantic sector (*14*). Temperature changes seen in AABW (*11*, *23*) are not apparent in ASBW (Fig.1C).

The observed trends in water mass properties have a number of implications. Changes in ASBW may influence Southern Ocean ecosystems through the distribution of salps and krill (*24*), although the impact of warming oceans on Antarctic krill is still debated (*25*) due to their spatially diverse lifecycles. We expect that megafaunal communities (*26*) on the shelf, in particular in the Bellingshausen and Amundsen Sea sectors, have experienced warmer and more frequent warm water intrusions of CDW. Further shoaling of CDW will increase the areas of the Antarctic shelf and the number of ice shelves that are influenced by offshore warming. This has the potential to increase the spatial extent of enhanced basal melt and to lead to irreversible retreat of a portion of the West Antarctic Ice Sheet, which will impact global sea level (*3*, *27*).

References and Notes:

1. A. Shepherd *et al.*, A Reconciled Estimate of Ice-Sheet Mass Balance. *Science* **338**, 1183–1189 (2012).
2. H. De Angelis, P. Skvarca, Glacier surge after ice shelf collapse. *Science* **299**, 1560–1562 (2003).
3. I. Joughin, B. E. Smith, B. Medley, Marine Ice Sheet Collapse Potentially Under Way for the Thwaites Glacier Basin, West Antarctica. *Science* **344**, 735–738 (2014).
4. E. Rignot, S. S. Jacobs, Rapid bottom melting widespread near Antarctic ice sheet grounding lines. *Science* **296**, 2020–2023 (2002).
5. H. D. Pritchard *et al.*, Antarctic ice-sheet loss driven by basal melting of ice shelves.

Nature **484**, 502–505 (2012).

6. A. A. Petty, D. L. Feltham, P. R. Holland, Impact of Atmospheric Forcing on Antarctic Continental Shelf Water Masses. *J. Phys. Oceanogr.* **43**, 920–940 (2013).

7. P. Spence *et al.*, Rapid subsurface warming and circulation changes of Antarctic coastal waters by poleward shifting winds. *Geophysical Research Letters* **41**, 2014GL060613 (2014).

8. S. S. Jacobs, C. F. Giulivi, Large multidecadal salinity trends near the Pacific-Antarctic continental margin. *J. Climate* **23**, 4508–4524 (2010).

9. H. H. Hellmer, O. Huhn, D. Gomis, R. Timmermann, On the freshening of the northwestern Weddell Sea continental shelf. *Ocean Sci.* **7**, 305–316 (2011).

10. S. T. Gille, Decadal-Scale Temperature Trends in the Southern Hemisphere Ocean. *J. Climate* **21**, 4749–4765 (2008).

11. S. G. Purkey, G. C. Johnson, Warming of Global Abyssal and Deep Southern Ocean Waters between the 1990s and 2000s: Contributions to Global Heat and Sea Level Rise Budgets*. *J. Climate* **23**, 6336–6351 (2010).

12. M. Azaneu, R. Kerr, M. M. Mata, C. A. E. Garcia, Trends in the deep Southern Ocean (1958-2010): Implications for Antarctic Bottom Water properties and volume export. *J. Geophys. Res. Oceans* **118**, 4213–4227 (2013).

13. S. Schmidtko, G. C. Johnson, J. M. Lyman, MIMOC: A global monthly isopycnal upper-ocean climatology with mixed layers. *J. Geophys. Res. Oceans* **118**, 1658–1672 (2013).

14. S. G. Purkey, G. C. Johnson, Antarctic Bottom Water Warming and Freshening: Contributions to Sea Level Rise, Ocean Freshwater Budgets, and Global Heat Gain. *J. Climate* **26**, 6105–6122 (2013).

15. P. R. Holland, R. Kwok, Wind-driven trends in Antarctic sea-ice drift. *Nature Geosci.* **5**, 872–875 (2012).

16. R. Bintanja, G. J. van Oldenborgh, S. S. Drijfhout, B. Wouters, C. A. Katsman, Important role for ocean warming and increased ice-shelf melt in Antarctic sea-ice expansion. *Nature Geosci.* **6**, 376–379 (2013).

17. A. L. Stewart, A. F. Thompson, Sensitivity of the ocean's deep overturning circulation to easterly Antarctic winds. *Geophysical Research Letters* **39**, L18604 (2012).

18. P. Dutrieux *et al.*, Strong Sensitivity of Pine Island Ice-Shelf Melting to Climatic Variability. *Science* **343**, 174–178 (2014).

19. H. H. Hellmer, F. Kauker, R. Timmermann, J. Determann, J. Rae, Twenty-first-century warming of a large Antarctic ice-shelf cavity by a redirected coastal current. *Nature* **485**,

225–228 (2012).

20. M. S. Dinniman, J. M. Klinck, E. E. Hofmann, Sensitivity of Circumpolar Deep Water transport and ice shelf basal melt along the west Antarctic Peninsula to changes in the winds. *J. Climate* **25**, 4799–4816 (2012).

21. C. Heuzé, K. J. Heywood, D. P. Stevens, J. K. Ridley, Southern Ocean bottom water characteristics in CMIP5 models. *Geophysical Research Letters* **40**, 1409–1414 (2013).

22. S. R. Rintoul, Rapid freshening of Antarctic Bottom Water formed in the Indian and Pacific oceans. *Geophysical Research Letters* **34**, L06606 (2007).

23. W. Zenk, E. Morozov, Decadal warming of the coldest Antarctic Bottom Water flow through the Vema Channel. *Geophysical Research Letters* **34**, L14607 (2007).

24. A. Atkinson, V. Siegel, E. Pakhomov, P. Rothery, Long-term decline in krill stock and increase in salps within the Southern Ocean. *Nature* **432**, 100–103 (2004).

25. A. Atkinson *et al.*, Oceanic circumpolar habitats of Antarctic krill. *Mar. Ecol. Prog. Ser.* **362**, 1–23 (2008).

26. L. J. Grange, C. R. Smith, P. Archambault, Ed. Megafaunal Communities in Rapidly Warming Fjords along the West Antarctic Peninsula: Hotspots of Abundance and Beta Diversity. *PLoS ONE* **8**, e77917 (2013).

27. E. Rignot, J. Mouginot, M. Morlighem, H. Seroussi, B. Scheuchl, Widespread, rapid grounding line retreat of Pine Island, Thwaites, Smith, and Kohler glaciers, West Antarctica, from 1992 to 2011. *Geophysical Research Letters* **41**, 3502–3509 (2014).

28. A. H. Orsi, T. Whitworth III, W. D. Nowlin, On the meridional extent and fronts of the Antarctic Circumpolar Current. *Deep-Sea Res. I* **42**, 641–673 (2003).

29. C. Amante, B. W. Eakins, ETOPO1 1 arc-minute global relief model: procedures, data sources and analysis. *NOAA Technical Memorandum NESDIS NGDC-24. National Geophysical Data Center, NOAA* (2009), doi:10.7289/V5C8276M.

30. W. S. Cleveland, S. J. Devlin, Locally Weighted Regression: An Approach to Regression Analysis by Local Fitting. *J. Am. Stat. Assoc.* **83**, 596–610 (1988).

Acknowledgments: All data used in this manuscript are publically available, data sources are detailed in the supplemental materials.

The authors thank all officers, crews and scientists involved in collecting and calibrating the data in the often harsh Southern Ocean environment, as well as everyone involved in making

the data publically available. The authors thank three anonymous reviewers for helpful discussions and feedback.

SS was partially funded by the German Federal Ministry for Education and Research (BMBF) project MiKlip. SS and KJH were funded by the NERC Antarctic Funding Initiative research grant GENTOO NE/H01439X/1. SA was supported by Grant-in-Aid for Scientific Research of the MEXT, Japan and Daiwa Foundation Small Grant. AFT was funded by NSF award OPP-1246460.

Figures:

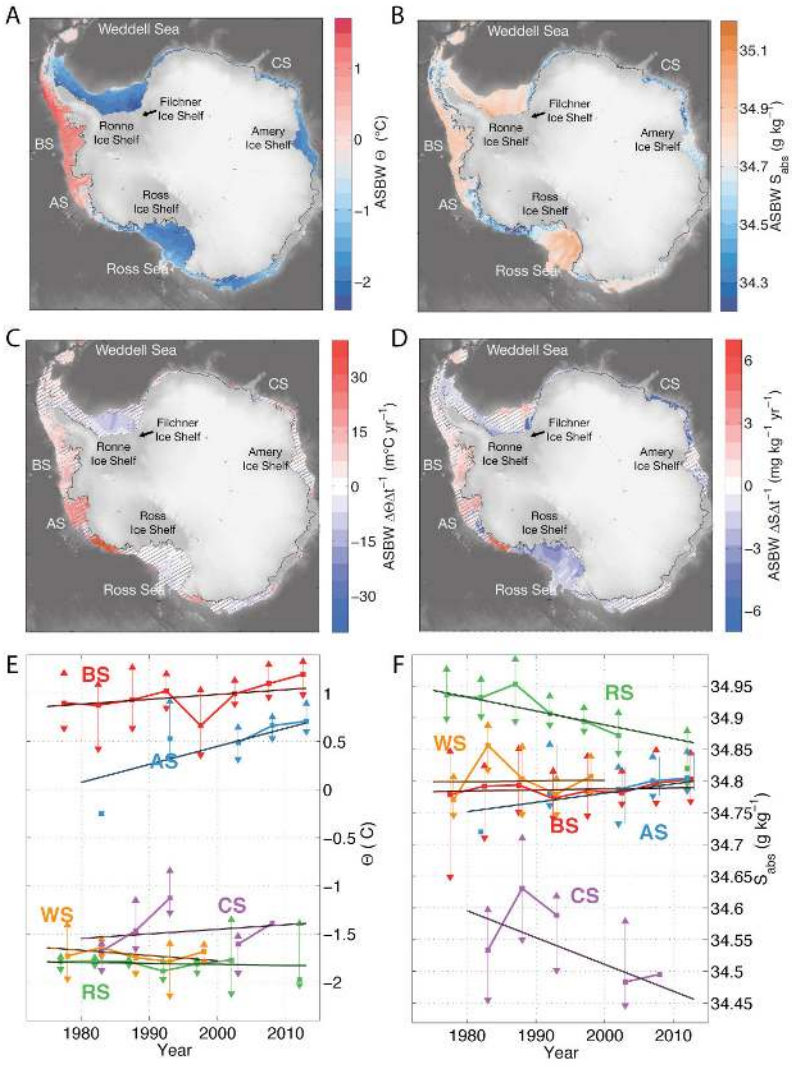

Fig. 1. Temporal means (A, B), linear trends (C, D) and multi-annual variability (E, F) in Antarctic Continental Shelf Bottom Water (ASBW). Conservative temperature (A, C) and absolute salinity (B, D) at the seabed for depths shallower than 1500m for the period 1975 to 2012. Trends (C, D) not statistically significant different from zero are hatched. (E, F) 5-year median properties since 1975, interquartile ranges and median trends for selected areas. Abbreviations used for surrounding seas are Bellingshausen Sea (BS), Amundsen Sea (AS), Ross Sea (RS), Cosmonaut Sea (CS) and Weddell Sea excluding the Antarctic Peninsula (WS).

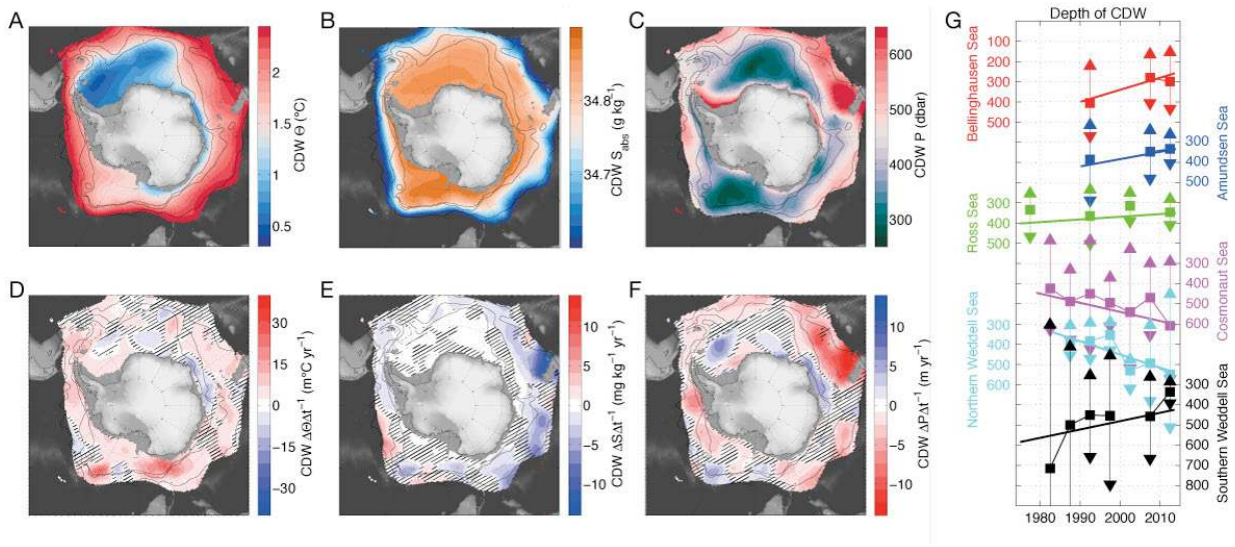

Fig. 2. Temporal means (A–C) and linear trends (D–F) in Circumpolar Deep Water (CDW). Conservative temperature (A, D), absolute salinity (B, E) and core depth (C, F) of CDW between 1975 and 2012. Trends not statistically significant different from zero are hatched. Fronts (*28*) related to the ACC are shown as black lines. Only regions where the ocean depth exceeds 1500 m and CDW cooler 2.8°C are shown. (G) Trends and data for selected locations.

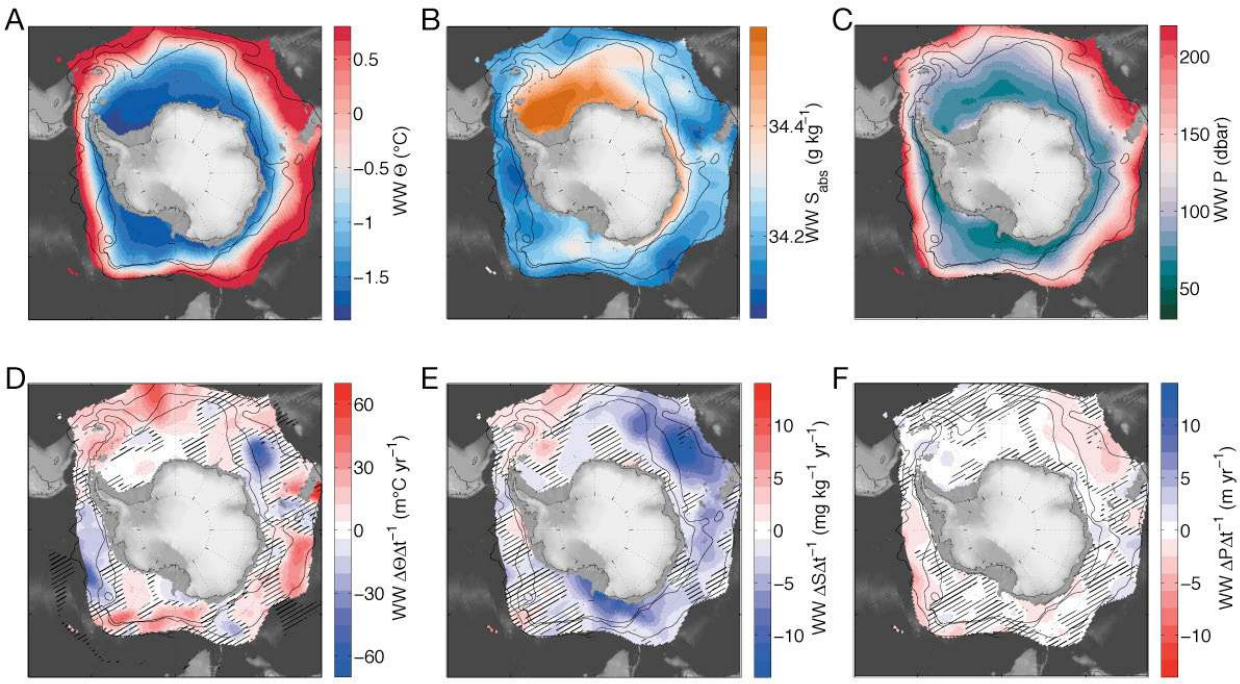

Fig. 3. Temporal means (A–C) and linear trends (D–F) in Winter Water (WW).

Conservative temperature (A, D), absolute salinity (B, E) and core depth (C, F) between 1975 and 2012. Trends not statistically significant different from zero are hatched. Fronts (*28*) related to the ACC are shown as black lines. Only regions where the ocean depth exceeds 1500 m and the underlying CDW is cooler than 2.8°C are shown.

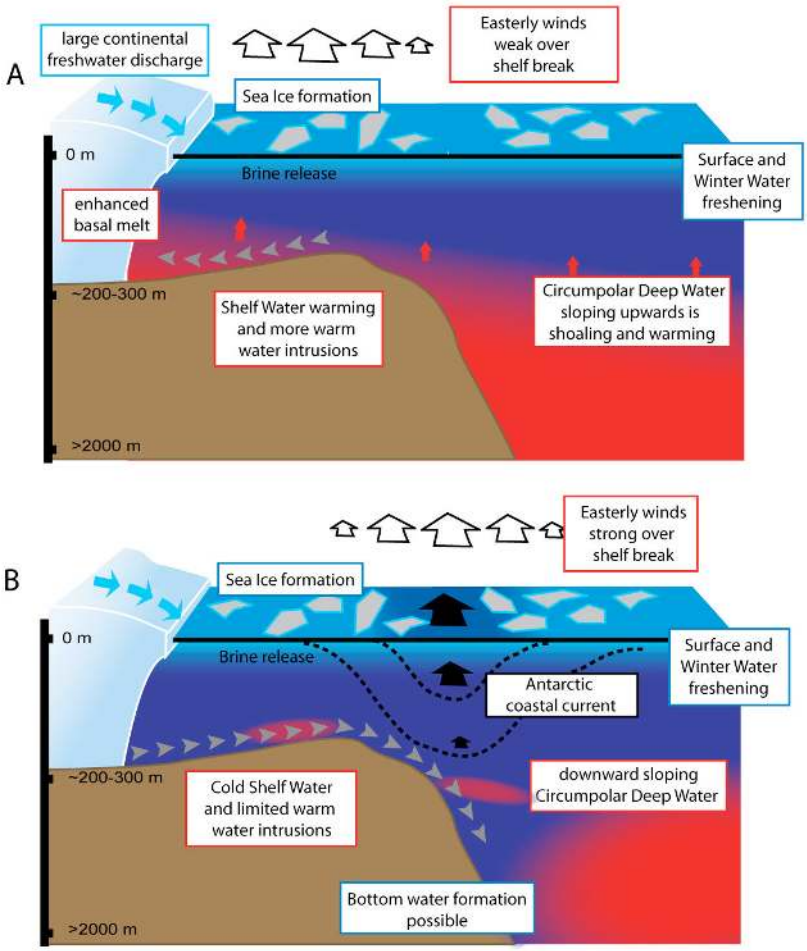

Fig. 4. Schematic differences of shelf water masses. A, Schematic of the Amundsen and Bellingshausen Seas with warm water at the bottom of the water column on the shelf. B, Schematic of the shelf in the Ross and Weddell Seas, with a strong Antarctic Slope Current.

Supplementary Materials:

Materials and Methods

Figures S1-S9

Tables S1

Materials and Methods:

We combined conductivity, temperature, depth (CTD) profiles from seven publicly available databases (Tab. S1) and mapped the properties of ASBW, WW, CDW and their associated trends since 1975. Due to limited data (Fig. S1) in this remote area, not all regions resolve the same period (Fig S2). Duplicates were avoided by checking for repeat profiles within 5 km and 25 h, allowing for rounding errors in latitude, longitude and time. In the rare case that 2 or more CTD casts were made within these temporal and spatial scales, we treat them as duplicates and only use one. When duplicate profiles were identified, the profile with the best vertical resolution was used. Profiles with a vertical resolution coarser than 20m were rejected; this filter is not applied to float data.

ASBW is defined using the deepest measurement in profiles within 30m of the bottom, or, in the absence of CTD altimeter data, within 150m of the ETOPO-1 bathymetry (*29*). This depth provides an estimate of uncertainty for the mapped bathymetry, since 5% of profiles exceed the bathymetry by up to 150 m. The cores of WW and CDW are defined by the conservative temperature (Θ) minimum below 40 m and the Θ maximum below the minimum, respectively.

ASBW data are mapped onto a 0.25°x0.125° grid for bathymetry shallower than 1500 m, while CDW and WW are mapped on a 0.5°x0.5° grid for bathymetry deeper than 1500 m. We apply the ETOPO-1 bathymetry for our analysis (*29*). For each grid point in our maps, the horizontal distance to data positions is derived by a Fast Marching algorithm (*13*). The algorithm uses a 300 m scaling in bathymetry difference and a minimum propagation of 0.1 on a 18x18 km grid for the speed map. This algorithm determines the along-path distance between the grid point to be mapped and data locations, including distance penalties for moving across bathymetry with different depths. Over the continental slope, the mapping is predominantly along bathymetric contours. Over flat bathymetry, the algorithm would result in a circular region of influence, however over rough, highly-variable terrain, the distances may be significantly longer in some directions (Fig. S7, S8). Only data at locations that can be reached with this marching algorithm are used.

Data are normally-weighted using an along-pathway horizontal scaling of 400 km. A vertical scaling of 200 dbar is applied for ASBW, but no vertical weighting is applied for WW and CDW. The vertical weighting for ASBW allows us to better differentiate ASBW properties and trends in troughs, canyons and other small-scale features on the shelf, which are not resolved in the ETOPO-1 data set (*29*). As a final step before mapping, an interquartile range (IQR) filter is applied to all parameters. Values more than twice the IQR below the first quartile or more than twice the IQR above the third quartile are rejected. We then apply a weighted least-squares

linear model (*30*) (LOESS) at each grid point to all data with positive weights larger than 10^{-3}. The model removes linear fits for longitude and latitude in the fast marching-derived coordinate system (*13*) as well as in depth for the shelf mapping. This LOESS model is used to determine the mean state and temporal trend of water mass properties. The spatial trend removal in the Fast Marching derived coordinate system accounts for across and along slope gradients for any resolved bathymetry (Fig. S7).

Statistically significant are trends that are larger than twice the 'estimated standard error' of the least squares solution. The 5-yr median properties of ASBW (Fig. 1E, F, S3, S5) are computed from the difference between raw data and the mapped properties, offset by the median mapped temperature and salinity.

Table S1. Data sources of used CTD data

Name	Website	Date accessed.	Comment
Argo floats	http://argo.ucsd.edu	05/2012	All data flagged good
World Ocean Database	http://www.nodc.noaa.gov/OC5/WOD09/pr_wod09.html	05/2013	All CTD data flagged good or probably good

Hydrobase 3	http://www.whoi.edu/science/PO/hydrobase/	06/2013	All CTD data used
Cliver and Carbon Hydrographic Database	http://cchdo.ucsd.edu/	01/2013	All CTD data available in netCDF format
Southern Ocean Database	http://woceatlas.tamu.edu/Sites/html/atlas/SOA_DATABASE.html	05/2013	All CTD data used
British Oceanographic Database	https://www.bodc.ac.uk/	06/2013	All data CTD flagged good
Pangaea database	http://www.pangaea.de/	05/2013	All Polarstern CTD data publically available

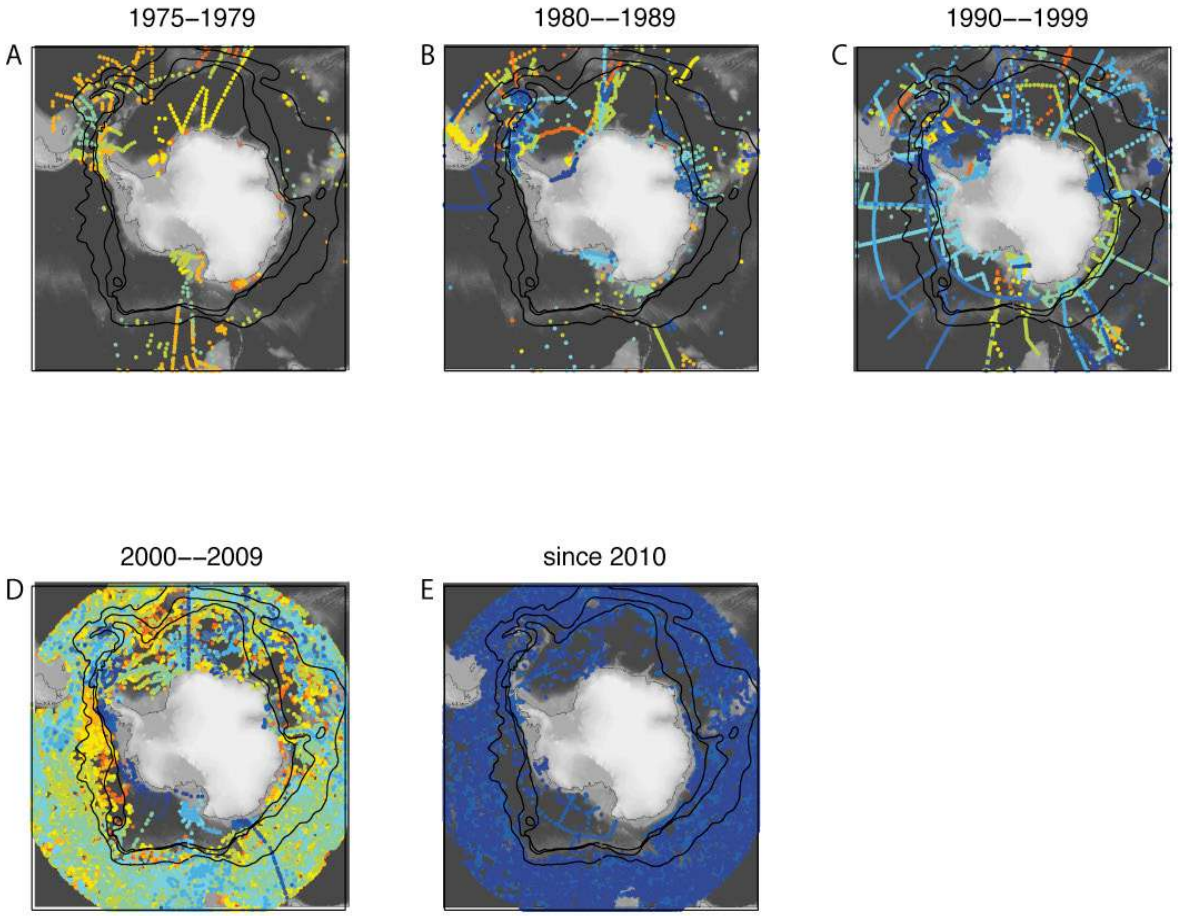

Fig. S1. Data coverage for each decade. A, Profile location from the period 1975–1979 and position of Antarctic Circumpolar Current fronts. B-E, similar to (A) for the successive decades. The individual years for each period are color-coded from blue (year 0) to red (year 9). Fronts (*28*) related to the ACC are shown as black lines.

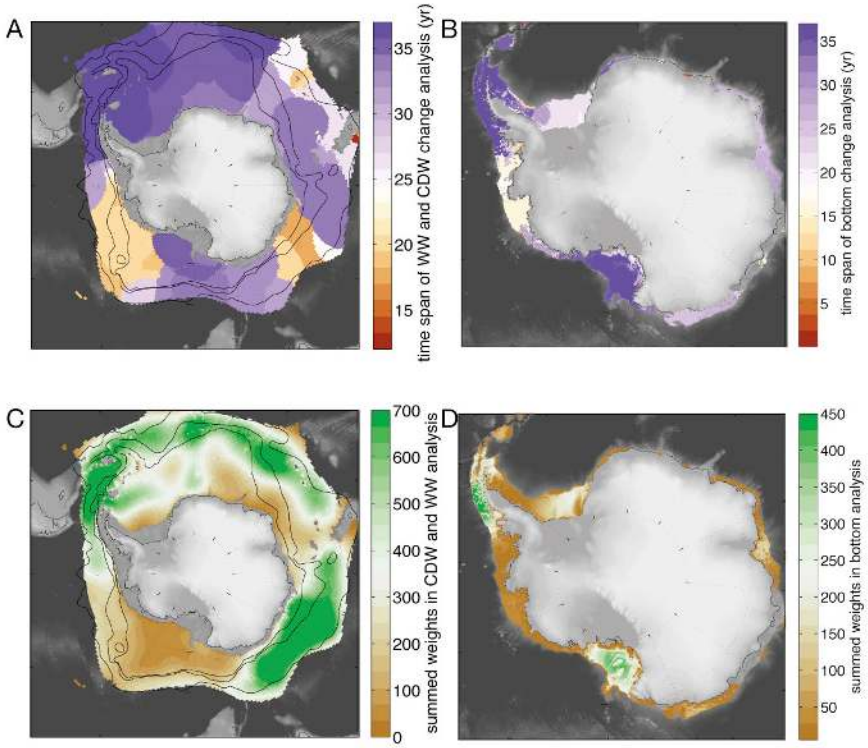

Fig. S2. Data density. A, Time span of linear trend computation for CDW and WW. B, similar to (A) for the bottom water analysis on the shelf. C, sum of weights used in Gaussian LOESS mapping at each grid point. D, similar to (C) for the on shelf bottom water analysis. Fronts (*28*) related to the ACC are shown as black lines.

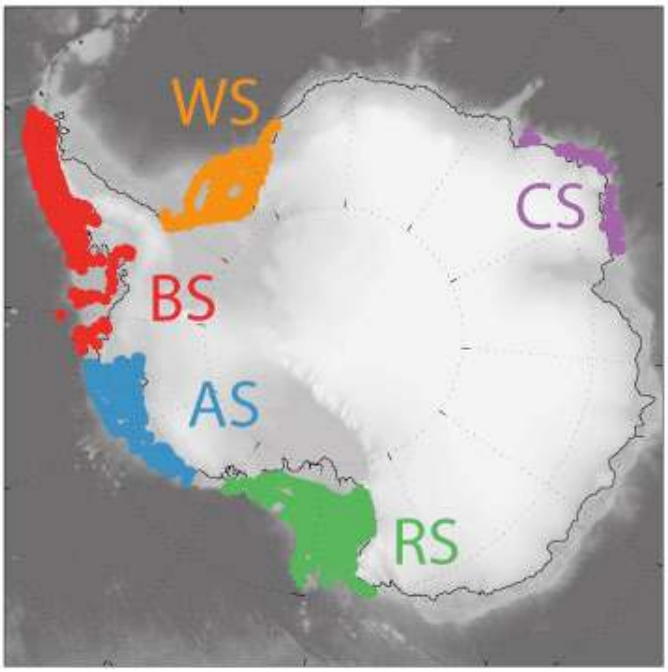

Fig. S3. Area extent and location of data used for the 5-yr bin average in Fig. 1E,F. Profile location from the period 1975–2012 for selected areas around Antarctica.

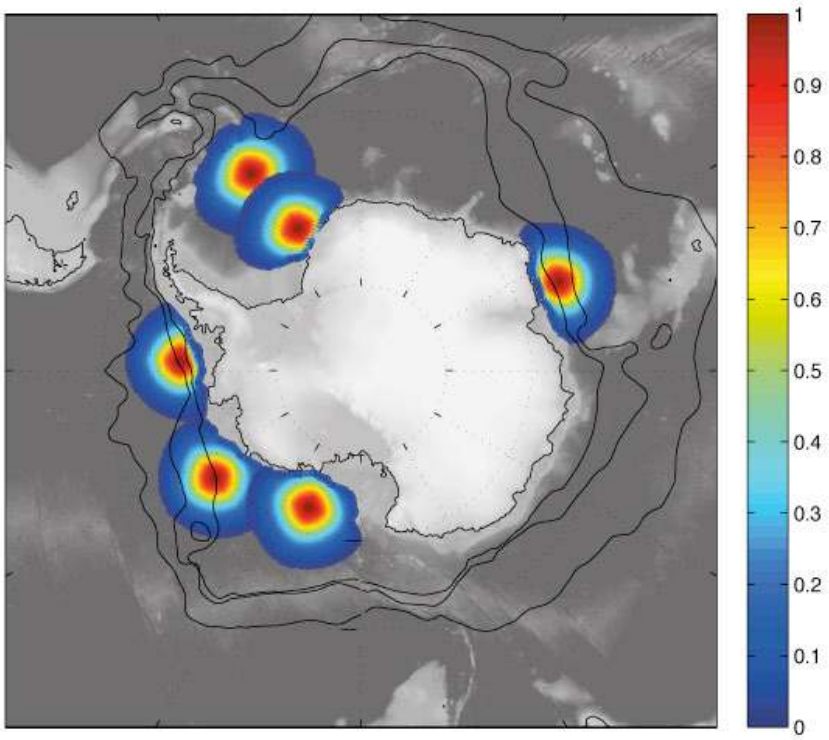

Fig. S4. Locations and distance weighting. Weights for LOESS mapping for the 6 regions used in Fig. 2G. The bathymetry-following mapping scheme does not include data from the shelf and reduces the weights rapidly under changing bathymetry. The center locations are assigned a weight of one with a Gaussian decay and a half folding scale of 400km. Fronts (*28*) related to the ACC are shown as black lines.

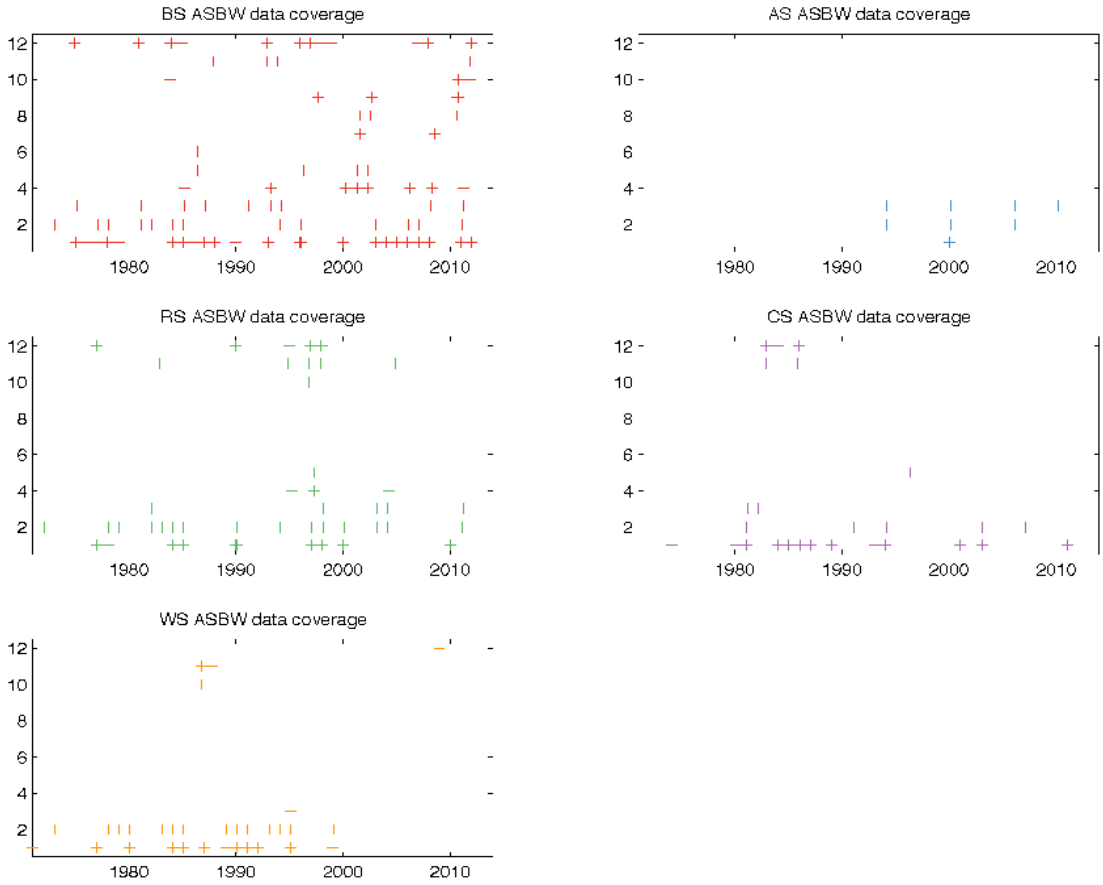

Fig. S5. Temporal data distribution as used for selected ASBW regions. Profile year and month of data for the 5 selected regions as shown in Fig. S5. These data are used for the 5-yr binned averages and inter quartile ranges in Fig. 1E,F.

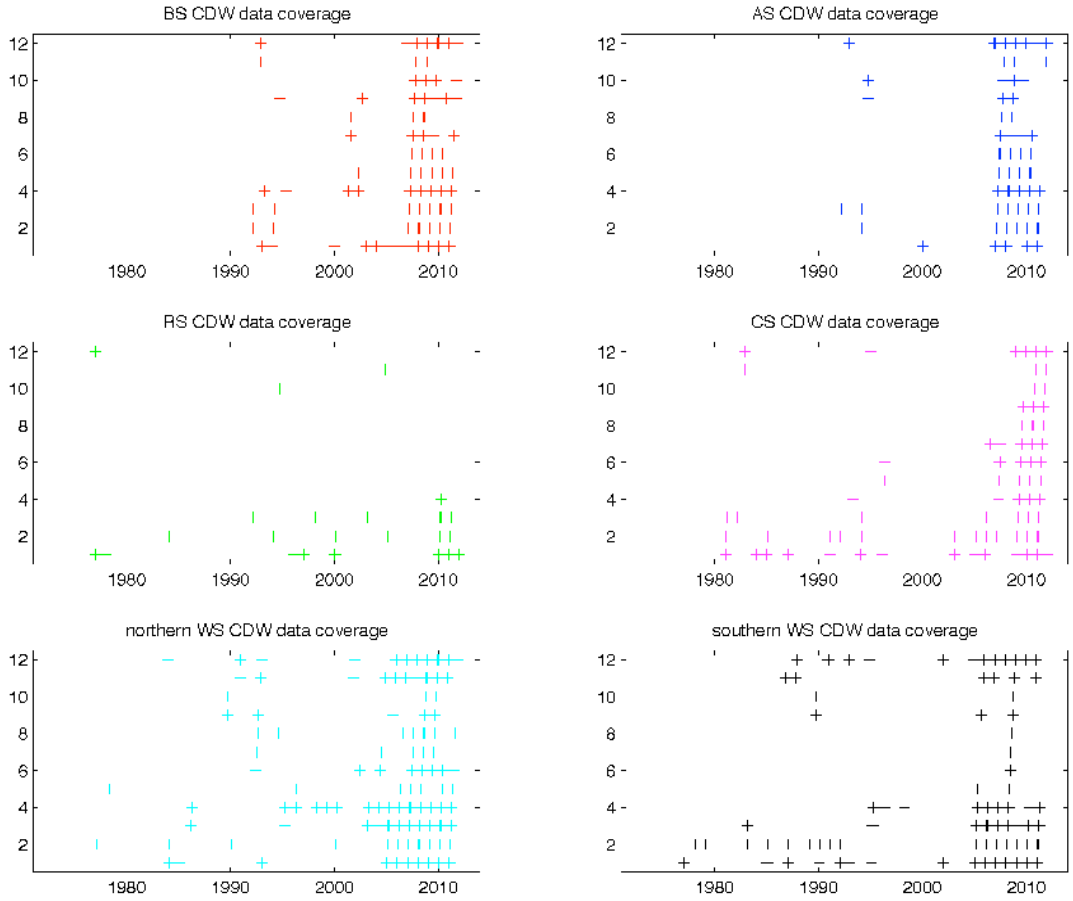

Fig. S6. Temporal data distribution as used for selected CDW regions. Profile year and month of data for the 6 selected regions as shown in Fig. S6. These data are used for the 5-yr binned averages and inter quartile ranges in Fig. 2G.

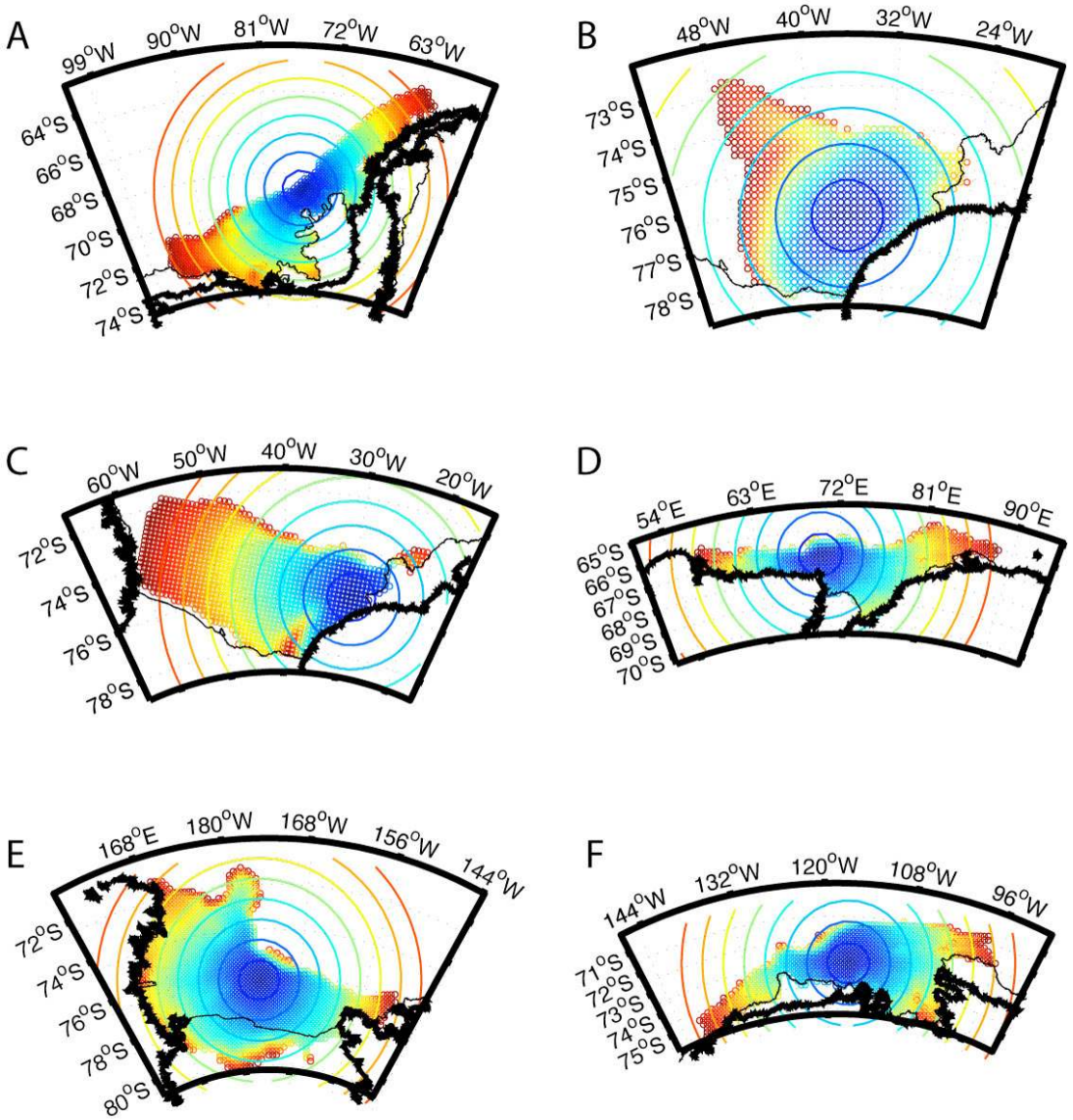

Fig. S7. Fast marching distances on the Antarctic shelf for selected shelf locations. The large circles indicate a circular influence region with contour spacing of 100km. Small circles indicate the locations reached by the fast marching algorithm and the assigned distance, using the same color coding as the large circles. The mapped regions are (A) the west Antarctic Peninsula, (B, C) the south western Weddell Sea for different locations, (D) the Cosmonaut Sea, (E) the Ross Sea and (F) the Amundsen Sea.

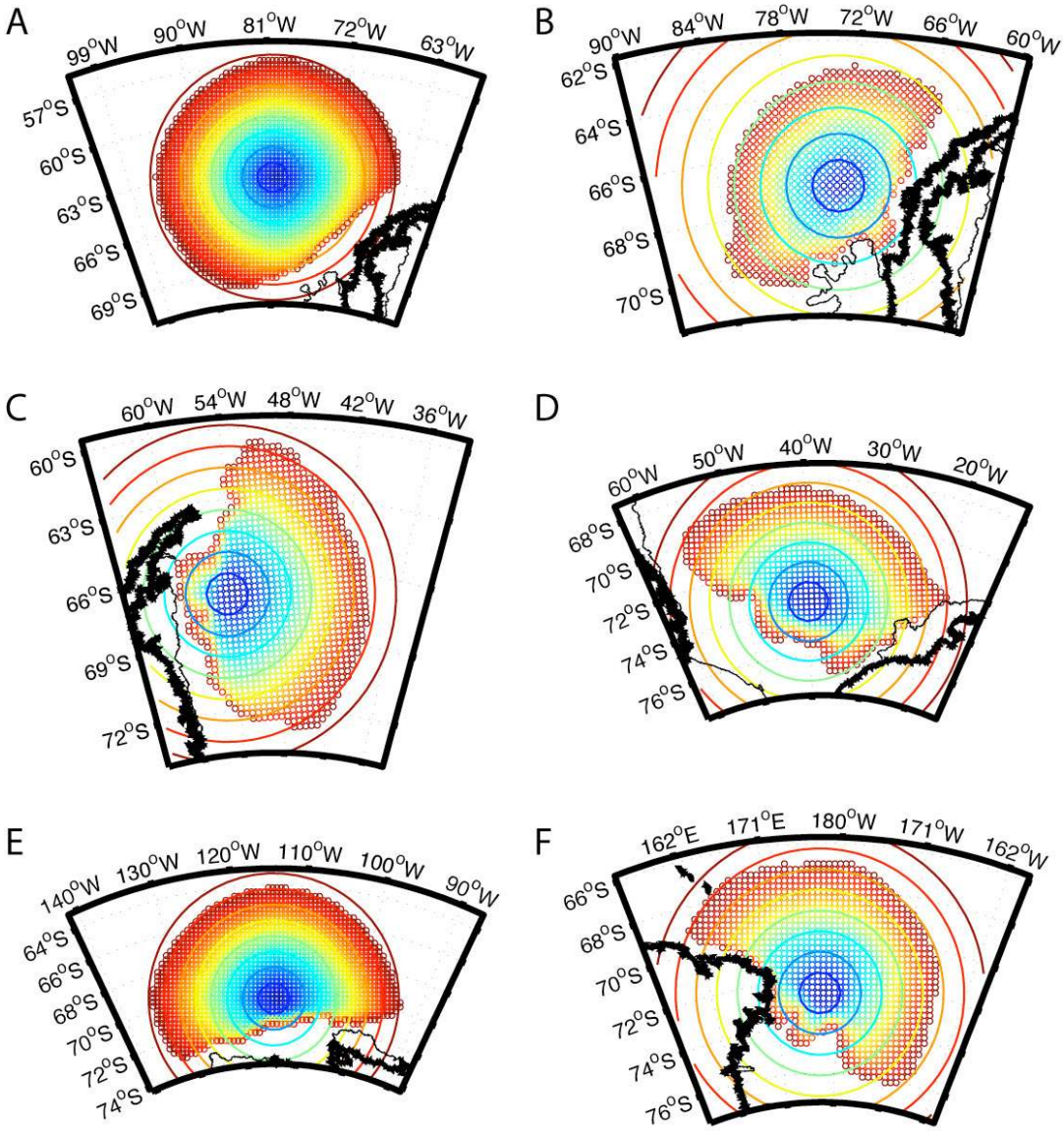

Fig. S8. Fast marching derived distances around Antarctic for selected continental slope locations. The large circles indicate a circular influence region with contour spacing of 100km. Small circles indicate the locations reached by the fast marching algorithm and the assigned distance, using the same color coding as the large circles. The mapped CDW regions are (A,B) Bellinghausen Sea, (C,D) Weddell Sea, (E) Amundsen Sea and (F) Ross Sea.

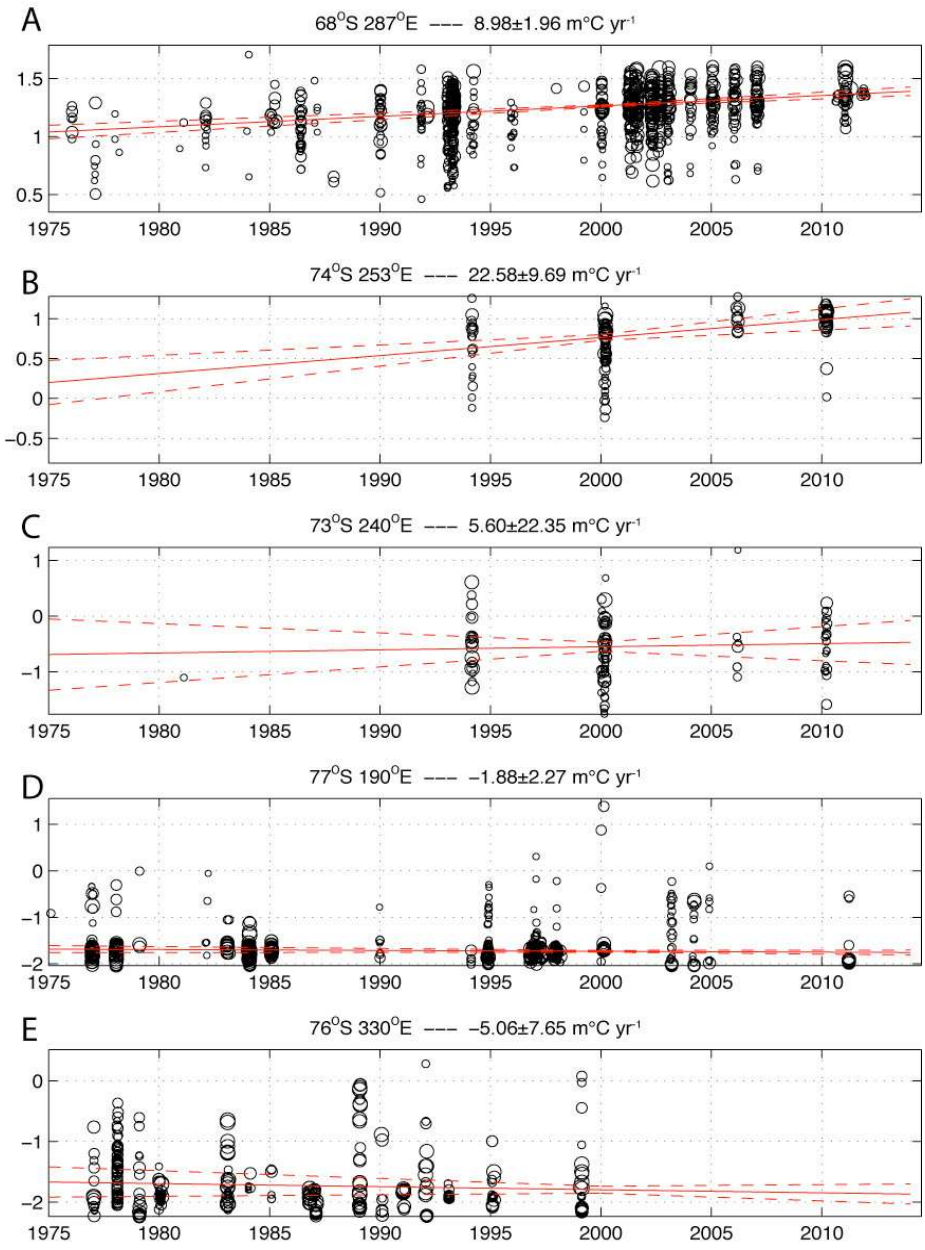

Fig. S9. Raw data distribution and trends for selected locations. Red lines indicate the trend (solid line) as well as uncertainty in the trend (dashed line). Uncertainties are given as twice the standard error. The trend is regarded as significant if it is larger than twice the standard error of the trend. Each circle is a data point, the size of the circle indicates the weight for the final mapping, using horizontal and vertical scaling (Fig. S7, methods). The regions are (A) Bellinghausen Sea, (B) Amundsen Sea – significant trend, (C) Amundsen Sea – non significant trend, (D) Ross Sea and (E) Weddell Sea.

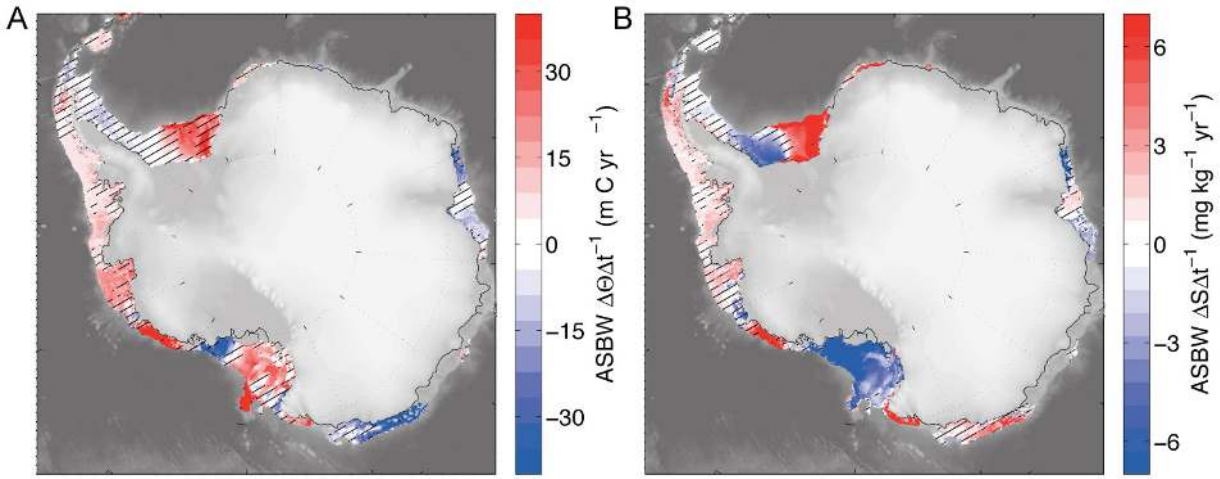

Fig. S10. Similar to Fig. 1C, D but for trends of ASBW using only data since 1990. Some areas, like the Weddell Sea shelf have very poor data coverage in recent decades, and trends shown might not represent the longer term change during this period, see Fig S1, S2, S5 for data coverage. Fig. 1C, D represent the ASBW long-term changes.

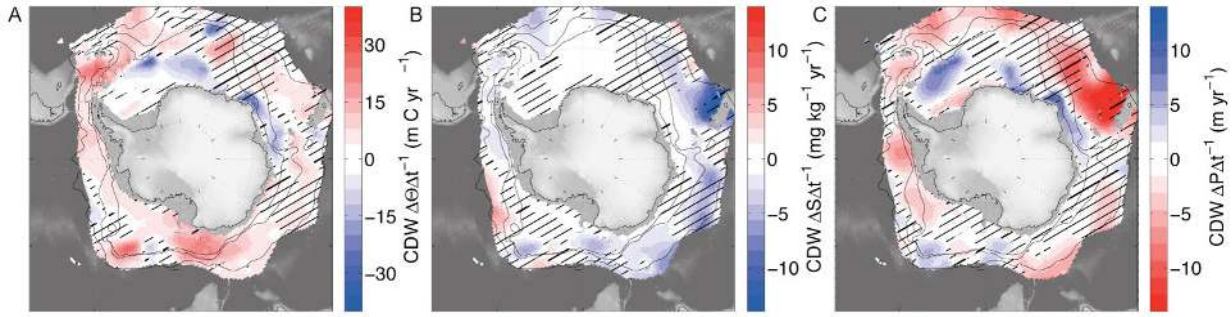

Fig. S11. Similar to Fig. 2 D–F but for trends of CDW using only data since 1990. Although the basic patterns are similar to those with data since 1975 (Fig. 2D–F) treat trends over this shorter time period with caution, see Figs. S1, S2, S6 for data coverage. Fig. 2D–F represent the CDW long-term changes. Fronts (*28*) related to the ACC are shown as black lines.